Atomic scattering factor for a spherical wave and near-field effects in x-ray fluorescence holography

Jianming Bai

Oak Ridge National Laboratory, Oak Ridge, Tennessee 37831, USA

A formula for calculating the atomic scattering factor for spherical x-ray waves is derived and used to solve the near field effects problem in x-ray fluorescence holography theory. A rigorous formalism to calculate the x-ray fluorescence hologram is then given so that quantitative structural information can be obtained from these holographic measurements.

I. INTRODUCTION

Atomic scattering factors (ASF's) are used in numerous crystallographic calculations. Their values are tabulated in the *International Tables for X-ray Crystallography*. These ASF's are defined under the assumption that both the x-ray source and the detector are far away from the scatterers so that both the incident and scattered x-ray can be represented by plane waves. This assumption is valid for most x-ray scattering experiments until the emergence of x-ray fluorescence holography (XFH) in recent years.[1–3] XFH, because of its unique view point, is a new technique with great potential in exploring the local arrangements of atoms. However, it needs further developments in two respects. First, because of the low signal/background ratio (typically 10^{-4} to 10^{-3}), it takes several days to collect data on a single hologram even with synchrotron radiation. The bottleneck is not the x-ray intensity but rather the detector speed. This problem will eventually be solved with the development of high-speed detectors. Secondly, the XFH is not yet a quantitative method because the real space field intensity image reconstructed using the well-known Barton algorithm[4] is deviated from the real electron charge density. This deviation may be caused by the angular dependence of the scattering power of atoms by a spherical wave. One way to solve this problem is to use a nonlinear least-square-fitting algorithm to accurately reconstruct the atomic arrangement; this requires a rigorous and forthright formalism to calculate the hologram. It is the object of this paper to derive the required formalism. In XFH, the fluorescence atoms inside the sample are used either as sources (in direct XFH) or as detectors [in inverse XFH, also called multiple energy x-ray holography (MEXH)]. The distance between the radiation source and scatterer, or the scatterer and the detector, is comparable to the size of the electron distribution of the scatterer. In this case, atomic scattering factors for a spherical wave should be used in the quantitative analysis for XFH. In most of the earlier works involving XFH calculation, a first-order approximation has been used.[5] This approximation assumes that the size of the core electron distribution of the scatterer is much smaller than the radius of the incident spherical wave front and is thus valid only for a pointlike scatterer. Tegze and Faigel investigated this problem by first formulating the hologram of a single electron and then calculating the hologram of an atom using numerical integrals over the charge density associated with the atom.[6] In this way they correctly calculated the effect of the wave front curvature at expense of the simple form of hologram equation as in Ref. 5. With correctly defined and calculated ASF for a spherical wave, as will be demonstrated in this paper, we can retain the simple form, which is simply a sum of products of the precalculated ASF and an exponential phase factor of the atoms contributing to the hologram, and include the effect of curved wave front. In the following section, the formula of the ASF for a spherical wave is first derived for a scalar field. The only assumption is that the source (or detector) is outside of the electron distribution of the scatterer, which is always satisfied in XFH experiments. A method to calculate the spherical wave ASF from the electron density distribution or from tabulated plane wave ASF's is developed. Its dependence on the atomic radii of the scatterer, the source-scatterer or scatterer-detector distance and the wavelength is then examined in the example calculations. Given the similarity between the definitions of x-ray and electron ASF, the same scheme can also be used to calculate the spherical wave ASF for electrons in the high-energy regime, which can be used to correct the "small atom approximation" in photoelectron spectroscopy.[7] In the third section, a XFH formula is derived from the theory of a vectorial field. A generalized form factor, which includes the near-field effects originates from both the vector nature of the electromagnetic field and the curved wave front, is obtained in terms of the spherical wave ASF and its derivatives.

II. ATOMIC SCATTERING FACTOR FOR A SPHERICAL WAVE

The x-ray fluorescence hologram is formed by the interference of the reference wave and the object waves. In direct XFH, the reference wave is the fluorescence radiation from the emitter atom and the object waves are the scattered fluorescence radiations from the surrounding atoms. In MEXF, the reference wave is the incident plane-wave and the object waves are scattered from the atoms surrounding the fluorescence emitter. The intensity of the fluorescence is a record of the interference pattern. In classical electrodynamics, the normalized x-ray fluorescence hologram is written as

$$\chi(\mathbf{k}) = -r_e \sum_i \int d\mathbf{r} \frac{\rho(|\mathbf{r}-\mathbf{r}_i|)}{r} e^{i(kr-\mathbf{k}\cdot\mathbf{r})} + \text{c.c.}, \quad (1)$$

where r_e is the classical electron radius and $\rho(\mathbf{r})$ is the electron charge density. The $\mathbf{r}$ is centered at the fluorescence emitter; $\mathbf{r}_i$'s are the centers of the scatterers and c.c. is the complex conjugation of the first term. To concentrate on the near-field effects caused by the atomic scattering factors, we consider here only the scalar wave equation. The near-field effects caused by the vectorial nature of electromagnetic wave will be explored later. Let $\mathbf{u}=\mathbf{r}-\mathbf{r}_i$ and assume that $u \ll r_i$, such that $r \approx r_i$ in the denominator and $r \approx r_i + \mathbf{r}_i \cdot \mathbf{u}/r_i$ in the phase term. We obtain the commonly used first approximation

$$\chi(\mathbf{k}) \approx -r_e \sum_i \frac{f_i(s_i)}{r_i} e^{i(kr_i-\mathbf{k}\cdot\mathbf{r}_i)} + \text{c.c.}, \quad (2)$$

with $f_i(s_i) = \int d\mathbf{u}\rho_i(u) e^{-i(\mathbf{k}-\mathbf{k}_i)\cdot\mathbf{u}}$, $s_i = |\mathbf{k}-\mathbf{k}_i|$, and $\mathbf{k}_i = k\mathbf{r}_i/r_i$.

Here f_i is just the ASF for plane wave x rays. This approximation does not take the curvature of the spherical wave front into account and is valid only when r_i is much larger than the radius of the scattering atom. This assumption is generally invalid for near neighbor atoms; a more accurate formula is needed.

We define the spherical ASF as

$$f_i^S(\theta_i, r_i) = r_i e^{-ikr_i+i\mathbf{k}\cdot\mathbf{r}_i} \int d\mathbf{r} \frac{\rho(|\mathbf{r}-\mathbf{r}_i|)}{r} e^{i(kr-\mathbf{k}\cdot\mathbf{r})}$$

$$= r_i e^{-ikr_i} \int d\mathbf{u}\rho(u) \frac{e^{ikr}}{r} e^{-i\mathbf{k}\cdot\mathbf{u}}. \quad (3)$$

By replacing the $f_i(s_i)$ in Eq. (2) with $f_i^S(\theta_i, r_i)$, one obtains the exact expression as given in Eq. (1).

The spherical wave term e^{ikr}/r can be expanded with spherical harmonics[8]

$$\frac{e^{ikr}}{r} = i4\pi k \sum_l (-1)^{l+m} j_l(ku_<) h_l^{(1)}(ku_>)$$

$$\times \sum_m Y_l^m(\Omega_{r_i}) Y_l^{-m}(\Omega_u), \quad (4)$$

and the plane wave term expanded as

$$e^{-i\mathbf{k}\cdot\mathbf{u}} = 4\pi \sum_{l',m'} (-i)^{l'}(-1)^{m'} j_{l'}(ku) Y_{l'}^{-m'}(\Omega_u) Y_{l'}^{m'}(\Omega_k). \quad (5)$$

Inserting Eqs. (4) and (5) into Eq. (3), we have

$$f_i^S(\theta_i, r_i) = (4\pi)^2 r_i k i e^{-ikr_i} \sum_{l,m} i^l(-1)^m Y_l^m(\Omega_{r_i}) Y_l^{-m}(\Omega_k)$$

$$\times \int_0^\infty u^2 j_l(ku) j_l(ku_<) h_l^{(1)}(ku_>)\rho(u)du$$

$$= 4\pi r_i k i e^{-ikr_i} \sum_l (2l+1) i^l P_l(\cos\theta_i)$$

$$\times \left[h_l^{(1)}(kr_i) \int_0^{r_i} j_l^2(ku)\rho(u)u^2 du \right.$$

$$\left. + j_l(kr_i) \int_{r_i}^\infty j_l(ku) h_l^{(1)}(ku)\rho(u)u^2 du \right]. \quad (6)$$

Here θ_i is the angle between $\mathbf{r}_i$ and $\mathbf{k}$. With knowledge of the atomic electron density, Eq. (6) can be calculated for any r_i value. However, in practice, it is more interesting to consider the situation when the source is outside of the electron distribution of the scattering atom. In this case, the second integration in Eq. (6) is zero. The plane wave ASF can be expanded with Legendre polynomial as

$$f(|\mathbf{k}'-\mathbf{k}|) = 4\pi \sum_l (2l+1) P_l(\cos\theta) \int_0^\infty j_l^2(ku)\rho(u)u^2 du, \quad (7)$$

with θ defined as the angle between $\mathbf{k}$ and $\mathbf{k}'$, Eq. (6) becomes

$$f_i^S(\theta_i, r_i) = \frac{kr_i}{2} e^{-ikr_i} \sum_l (2l+1) i^{l+1} P_l(\cos\theta_i) h_l^{(1)}(kr_i)$$

$$\times \int_0^\pi P_l(\cos\theta) f_i[2k\sin(\theta/2)]\sin\theta d\theta. \quad (8)$$

One can easily verify Eq. (8) by assuming that r_i is very large or that $\rho(u)$ is a delta function (so $f_i=z$), in both the cases $f_i^S(\theta_i, r_i)$ will degenerate into $f_i(s_i)$. The physical meaning of Eq. (8) is that the scattering power of an atom for a spherical wave can be represented by a weighted sum of plane wave ASF with the same wavelength in all directions.

When Eq. (8) is applied to a very small r_i with tabulated plane wave ASF values, e.g., when r_i equals 2.4825 Å, which is the nearest neighbor distance in a bcc iron crystal, the series in Eq. (8) is not convergent. This is because for free atoms the electron density continues beyond the nearest neighbor distance in their crystal form. From Fig. 1, one can see that for an iron atom a small part of the electron distribution in the $4s$ shell is outside of its first neighbor distance in the crystal. Therefore, the simple form of spherical wave ASF in Eq. (8) is not valid in this case since the first integral in Eq. (6) cannot be extended to infinity. Calculations show that Eq. (8) can be safely used for r_i greater than twice the nearest neighbor distance for most elements. Spherical wave ASF can be calculated from Eq. (6) if the radial electron density is known. Even though the radial atomic electron densities can be very well calculated based on the shell model of atoms, their values are not conveniently available.
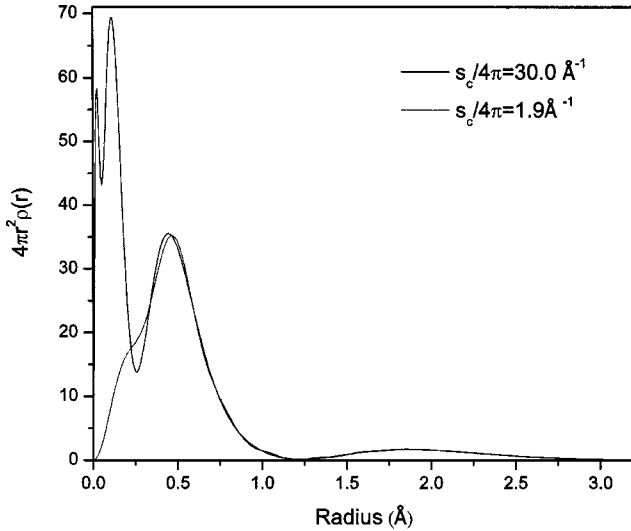
FIG. 1. Partial electron distributions of atom iron calculated with Eq. (13). The plane wave ASF for iron used here is based on an analytical interpolation of one-electron wave functions built to approximate the solution to Hartree-Fock equationsand is valid for the entire range of s (Ref. 14). For a cutoff s of 30 Å^{-1}, the partial electron distribution calculated (solid line) is describes almost completely the full electron distribution of atomic iron.

It will be useful to have a formalism to calculate the spherical ASF with plane wave ASF values which are experimentally measurable physical parameters. It is well known that the plane ASF is simply a three-dimensional Fourier image of the atomic electron distribution. For a spherical radial electron density model, we have

$$f(s) = 4\pi \int_0^\infty \rho(r) \frac{\sin(sr)}{sr} r^2 dr \qquad (9)$$

and

$$\rho(r) = \frac{1}{2\pi^2 r} \int_0^\infty f(s)\sin(sr)s\, ds. \qquad (10)$$

The tabulated ASF values in the *International Tables for Crystallography*[9] are only available in the range of $s/4\pi$ from 0.0 to 6.0 Å^{-1}. Evaluation of an accurate electron distribution requires a wider s range. However, what we need for evaluating the spherical ASF from Eq. (6) is the tail of the atomic electron density far from its nucleus which is determined by the low s values of $f(s)$. We can calculate a partial electron density by constructing a partial ASF, $f_c(s)$, which is defined as

$$f_c(s) = ae^{-bs^2} \text{ for } s \leq s_c \text{ and } f_c(s) = f(s) \text{ for } s > s_c. \qquad (11)$$

Here s_c is the cutoff value of s. The a and b are defined by setting the value and first derivative of $f_c(s)$ equal to those of $f(s)$ at the cutoff s_c:

$$a = f(s_c)e^{bs_c^2}, \quad b = -\frac{f'(s_c)}{2s_c f(s_c)}. \qquad (12)$$

The $f_c(s)$ as defined corresponds only to the electron density

close to the nucleus so that the partial electron density given by

$$\rho_p(r) = \frac{1}{2\pi^2 r} \int_0^{s_c} [f(s) - f_c(s)]\sin(sr)s\, ds$$

$$= \frac{1}{2\pi^2 r} \int_0^\infty [f(s) - f_c(s)]\sin(sr)s\, ds \qquad (13)$$

will give the correct electron density for large r's. Figure 1 shows that the partial electron density calculated with a cutoff $s_c/4\pi = 1.9$ Å^{-1} accurately represents the entire $4s$ electron distribution for an iron atom. The partial ASF $f_c(s)$ represents only the electron distribution very close to the nucleus and can now be used in Eq. (8). The partial electron density which can be calculated with Eq. (13) with known plane wave ASF up to $s = s_c$ can be used in Eq. (6) to account for the contributions to the spherical ASF other than those from $f_c(s)$. Now the spherical wave ASF is given as

$$f_i^S(\theta_i, r_i) = \frac{kr_i}{2}e^{-ikr_i}\sum_l (2l+1)i^{l+1}P_l(\cos\theta_i)c_l(k,r_i) \qquad (14)$$

and

$$c_l(k,r_i) = h_l^{(1)}(kr_i)\int_0^\pi P_l(\cos\theta)f_c\left[2k\sin\left(\frac{\theta}{2}\right)\right]\sin\theta\, d\theta$$

$$+ 8\pi\left(h_l^{(1)}(kr_i)\int_0^{r_i} j_l^2(ku)\rho_p(u)u^2 du \right.$$

$$\left. + j_l(kr_i)\int_{r_i}^\infty j_l(ku)h_l^{(1)}(ku)\rho_p(u)u^2 du \right). \qquad (15)$$

Equation (15) can be used to calculate the spherical wave ASF for any physically meaningful r_i values. The cutoff value $s_c/4\pi$ must be greater than $1/\lambda$ and less than the higher limit of the effective range of plane wave ASF value. Since 0 to 2.0 Å^{-1} is the effective range of the widely used analytical representation of the plane wave ASF, the cutoff value of 1.9 Å^{-1} used in the above example is a good choice for x rays of energies less than 23 keV. In a crystal, the outmost electron distribution of an atom will be redistributed due to the neighbor atoms. Thus, the spherical symmetry is only approximately valid for the outmost electrons. Calculation shows that the contribution from the electron distribution outside r_i, which is given by the second integration in Eq. (15), is negligibly small (Fig. 2), thus the error caused by the spherical symmetry approximation should be small. It is well established that for plane wave ASF the x-ray reflection intensities are well represented by the free atom values of the form factors and are not very sensitive to the small redistributions of the electrons.[10]

As an example, the spherical ASF's were calculated for an iron atom with different r_i (Fig. 3) and for different x-ray energies (Fig. 4). With the exception of the 40 kev curves, a cutoff $s_c/4\pi = 1.9$ Å^{-1} and the four-Gaussian analytical representation of plane ASF by Doyle and Turner[11] were used. For the 40 keV curves, a cutoff $s_c/4\pi = 3.5$ Å^{-1} and the five-Gaussian analytical representation of plane wave ASF by Waasmaier and Kirfel,[12] which has an effective range from 0 to 6.0 Å^{-1}, were used. The calculations show that the
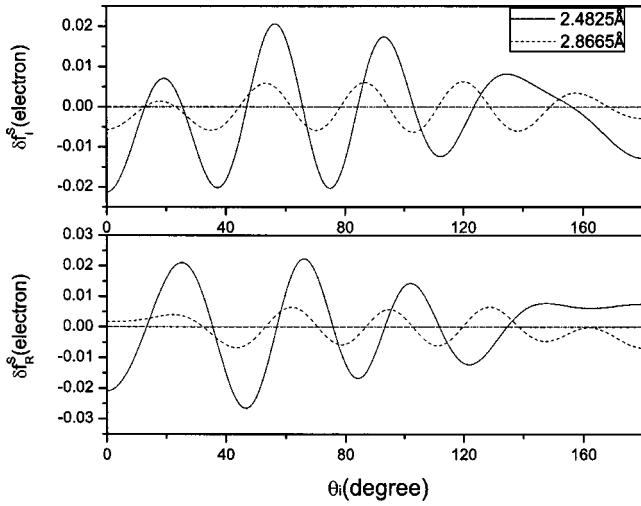
FIG. 2. The imaginary (top) and real part (bottom) of the contributions to the spherical wave ASF for iron from the electron distributions beyond its first and second neighbor distance. The x-ray energy is 8 keV.

real parts (and the magnitude) of the spherical wave ASF's are about 10 to 20 % less than the plane wave ASFs for the first neighbor scatterers around the forward scattering direction ($\theta_i = 0$) and approach the plane wave ASF values at high angles. This correction is mainly due to the curved wave front. The plane wave ASF will reach the electron number Z in forward scattering because in this direction the complete electron density distribution in the atom has the same phase. This will never happen for a spherical wave. The fact that the real part of the spherical wave correction vanishes at higher angles can be understood by looking at Eq. (9). The contribution to the ASF is mainly from electrons near the nucleus of the scattering atom for high s since the function $\sin(sr)/sr$ acts as a δ function for high s. The curved wave front correction is small for inner shell electrons. The imaginary part of the spherical ASF has a positive value about 10 to 20 % of the atomic electron number and approaches a small negative constant at higher angles. This correction is a combination of the curved wave front effect and the $1/r$ dependence of the spherical wave amplitude. The $1/r$ weight in the electron distribution integration makes the apparent scatterer position closer to the source. Hence this contributes a negative phase shift. This shift does not depend on the scattering angle. The overall effect of the spherical wave ASF correction is that when the scatterer is between the source atom and the detector, it is 10 to 20 % less in scattering power and apparently shifts away from the source. When the scatterer is on the opposite side of the source relative to the detector, it has an apparent position shift towards the source. The curved wave front correction is larger for shorter source-scatterer distance (Figs. 2 and 3) and higher x-ray energies (Fig. 4) as shown. Figure 2 shows the contribution to the spherical ASF from the electrons beyond r_i. The largest contribution is for the first neighbor scatterers and is less than 0.03 electrons for iron at 8 keV. The outer shell electron contribution is less for higher energies (not shown).
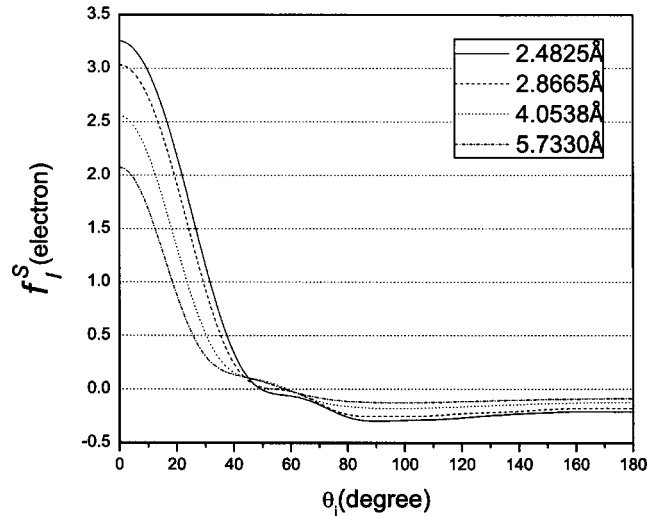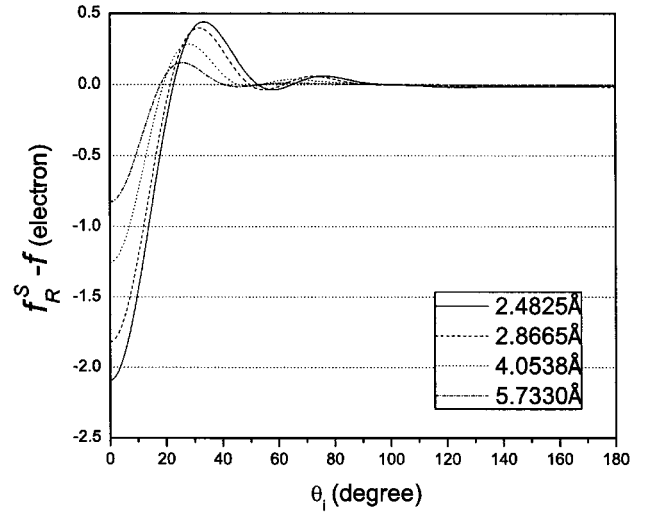

FIG. 3. (Color online) The difference between the real part of the spherical wave ASF and the plane wave ASF (top) and the imaginary part of the spherical wave ASF (bottom) for iron calculated with r_i equal to its first, second, third and fourth neighbor distance at 8 keV.

III. NEAR FIELD EFFECTS DERIVED FROM VECTOR THEORY

In addition to the near field effects caused by the spherical wave front, there are also near field effect terms caused by the vector property of the x-ray wave. In Ref. 5 these terms were considered under the plane wave approximation. Now with the spherical ASF, we can give a more accurate expression for these terms. In direct XFH, at the observation point **r** far away from the object, the total electric wave field is given by[13]

$$\mathbf{E}(\mathbf{r}) = \nabla \times \nabla \times [g(r)\mathbf{p}] - \frac{r_e}{k^2} \nabla$$

$$\times \nabla \times \int \mathbf{dr}' \{g(|\mathbf{r}-\mathbf{r}'|)\rho(\mathbf{r}')\nabla' \times \nabla' \times [g(r')\mathbf{p}]\},$$
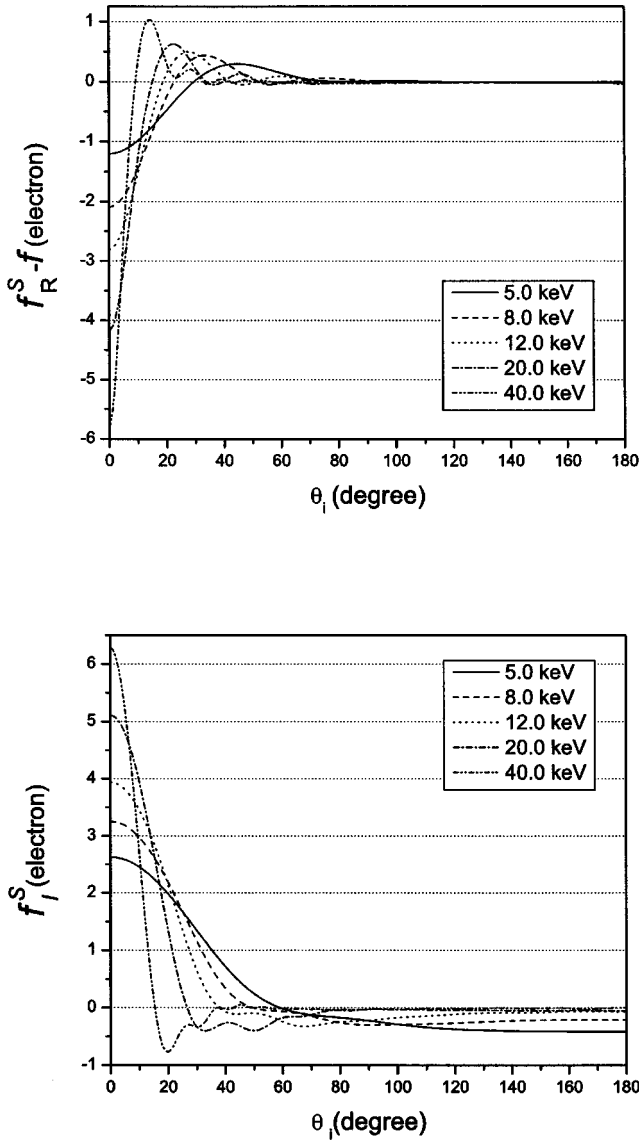
(16)

FIG. 4. (Color online) X-ray energy dependence of the ASF for a spherical wave. Top: real part of the spherical ASF minus the plane ASF. Bottom: imaginary part.

where $g(r) = \exp(ikr)/r$ and $\mathbf{p}$ is the electric dipole moment at $\mathbf{r} = 0$. Assuming $r \gg r'$, we can simplify Eq. (16) to

$$\mathbf{E}(\mathbf{r}) = k^2 g(r)\mathbf{n} \times \left[\mathbf{p} - \frac{r_e}{k^2} \sum_i e^{-i\mathbf{k}\cdot\mathbf{r}_i} \nabla_i \times \nabla_i \right.$$

$$\times \left(\int d\mathbf{u}\, e^{-i\mathbf{k}\cdot\mathbf{u}} \rho(u) g(|\mathbf{r}_i + \mathbf{u}|) \mathbf{p} \right) \right] \times \mathbf{n}$$

$$= k^2 g(r)\mathbf{n} \times \left[\mathbf{p} - \frac{r_e}{k^2} \sum_i e^{-i\mathbf{k}\cdot\mathbf{r}_i} \nabla_i \times \nabla_i \right.$$

$$\left. \times [\eta(r_i,\theta_i)\mathbf{p}] \right] \times \mathbf{n}. \tag{17}$$

Here $\mathbf{n} = \mathbf{r}/r$, $\eta(r_i,\theta_i) = g(r_i) f_i^S(\theta_i, r_i)$, and the sum is over all surrounding atoms. This leads to an expression for the hologram

$$\chi(\mathbf{k}) = \sum_i \chi_i(\mathbf{k})$$

with $\quad \chi_i(k) = -\dfrac{r_e}{k^2} e^{-i\mathbf{k}\cdot\mathbf{r}_i} \nabla_i \times \nabla_i \times [\, \eta(r_i,\theta_i)\mathbf{p}] \cdot \mathbf{p}_n / \mathbf{p}\cdot\mathbf{p}_n$

$$+ \text{c.c.} \tag{18}$$

Here $\mathbf{p}_n = \mathbf{n} \times \mathbf{p} \times \mathbf{n} = \mathbf{p} - (\mathbf{n}\cdot\mathbf{p})\mathbf{n}$. After some tedious but straightforward vector algebra, we have

$$\chi_i(\mathbf{k}) = -\frac{r_e}{k^2} e^{-i\mathbf{k}\cdot\mathbf{r}_i} \left\{ -\mathbf{p}\cdot\mathbf{p}_n \nabla_i^2 \, \eta(r_i,\theta_i) \right.$$

$$+ (\mathbf{p}\cdot\hat{\mathbf{r}}_i)(\mathbf{p}_n\cdot\hat{\mathbf{r}}_i) \frac{\partial^2}{\partial r_i^2} \eta(r_i,\theta_i) + [(\mathbf{p}\cdot\hat{\mathbf{r}}_i)(\mathbf{p}_n\cdot\hat{\theta}_i)$$

$$+ (\mathbf{p}_n\cdot\hat{\mathbf{r}}_i)(\mathbf{p}\cdot\hat{\theta}_i)] \frac{\partial}{\partial r_i}\left(\frac{1}{r_i}\frac{\partial}{\partial\theta_i} \right) \eta(r_i,\theta_i)$$

$$+ (\mathbf{p}\cdot\hat{\theta}_i)(\mathbf{p}_n\cdot\hat{\theta}_i) \frac{1}{r_i}\left(\frac{\partial}{\partial r_i} + \frac{1}{r_i}\frac{\partial^2}{\partial\theta_i^2} \right) \eta(r_i,\theta_i)$$

$$+ (\mathbf{p}\cdot\hat{\varphi}_i)(\mathbf{p}_n\cdot\hat{\varphi}_i) \frac{1}{r_i}\left(\frac{\partial}{\partial r_i} \right.$$

$$+ \left. \left. \frac{1}{r_i\tan(\theta_i)}\frac{\partial}{\partial\theta_i} \right) \eta(r_i,\theta_i) \right\} \Big/ \mathbf{p}\cdot\mathbf{p}_n + \text{c.c.} \tag{19}$$

For direct XFH, the electric dipole moment $\mathbf{p}$ is averaged in 4π solid angles since the fluorescence radiation is unpolarized. So we now have

$$\chi_i(\mathbf{k}) = -r_e e^{-i\mathbf{k}\cdot\mathbf{r}_i} \left\{ \eta(r_i,\theta_i)(1+\cos^2\theta_i)/2 \right.$$

$$+ \frac{1}{2k^2}\left[\frac{3\cos^2\theta_i - 1}{r_i}\frac{\partial}{\partial r_i}\eta(r_i,\theta_i) \right.$$

$$+ \frac{\cos(2\theta_i)}{r_i^2}\frac{\partial^2}{\partial\theta_i^2}\eta(r_i,\theta_i)$$

$$+ \frac{\sin(2\theta_i)}{r_i}\frac{\partial^2}{\partial r_i \partial\theta_i}\eta(r_i,\theta_i)$$

$$+ \left. \left. \frac{1-3\sin^2\theta_i}{r_i^2\tan\theta_i}\frac{\partial}{\partial\theta_i}\eta(r_i,\theta_i) \right] \right\} + \text{c.c.} \tag{20}$$

In deriving Eq. (20), we note that the function $\eta(r_i,\theta_i)$ satisfies the Helmholtz differential equation $\nabla_i^2\eta + k^2\eta = 0$. The derivatives of $\eta(r_i,\theta_i)$ can be calculated using Eq. (8). For example, $\partial\eta(r_i,\theta_i)/\partial\theta_i = k/2\sum_l(2l+1)i^{l+1}P_l^1(\cos\theta_i)h_l^{(1)}(kr_i)\int_0^\pi P_l(\cos\theta)f_i[2k\sin(\theta/2)]\sin\theta d\theta$. Here $P_l^1(\cos\theta_i)$ is an associated Legendre polynomial of order l and degree 1.

For MEXH, we assume the incident x-ray wave is polarized and the $\mathbf{E}$ vector is perpendicular to $\mathbf{k}$ and surface normal of the sample, as in the case of synchrotron radiation, then we have

$$\chi_i(\mathbf{k}) = -r_e e^{-i\mathbf{k}\cdot\mathbf{r}_i}\left\{ \eta(r_i,\theta_i)(1-\sin^2\theta_i\cos^2\varphi_i)\right.$$

$$+\frac{1}{k^2}\left[\frac{1-3\sin^2\theta_i\cos^2\varphi_i}{r_i}\frac{\partial}{\partial r_i}\eta(r_i,\theta_i)\right.$$

$$+\frac{\cos(2\theta_i)\cos^2\varphi_i}{r_i^2}\frac{\partial^2}{\partial\theta_i^2}\eta(r_i,\theta_i)$$

$$+\frac{\sin(2\theta_i)\cos^2\varphi_i}{r_i}\frac{\partial^2}{\partial r_i\partial\theta_i}\eta(r_i,\theta_i)$$

$$\left.\left.+\frac{1-\cos^2\varphi_i(1+3\sin^2\theta_i)}{r_i^2\tan\theta_i}\frac{\partial}{\partial\theta_i}\eta(r_i,\theta_i)\right]\right\}+\text{c.c.}$$

$$(21)$$

If the incident beam is unpolarized, Eq. (21) needs to be averaged over φ_i and will be the same as Eq. (20). In Eqs. (20) and (21), the $\chi_i(\mathbf{k})$'s dependence on the direction of $\mathbf{k}$ is through θ_i, which is the angle between $\mathbf{k}$ and $\mathbf{r}_i$; and φ_i, the angle between $\mathbf{p}$ and $\mathbf{r}_i-(\mathbf{n}\cdot\mathbf{r}_i)\mathbf{n}$. They can be expressed in terms of the spherical coordinates of $\mathbf{k}$ (θ,φ) and $\mathbf{r}_i(\theta_i',\varphi_i')$ in a coordinator system fixed on the sample

$$\cos\theta_i = \cos\theta\cos\theta_i' + \sin\theta\sin\theta_i'\cos(\varphi-\varphi_i'),$$

$$\cos\varphi_i = \sin(\varphi-\varphi_i')\sin\theta_i'/\sin\theta_i. \qquad (22)$$

Combing Eqs. (18), (20), (21), and (22), the x-ray fluorescence holograms can be calculated with consideration of complete near field effects. Figure 5 shows a calculated $\chi_i(\theta,\varphi=0)$ curve for a single emitter-scatterer pair of iron atoms. The fluorescence emitter atom is at the origin while the scatterer is at 2.4825 Å along the x axis (e.g., $\theta_i'=\varphi_i'=0$). The calculation shows that at an x-ray energy of 6.4 keV, the corrections due to the two kinds of the near field effects are comparable. At x-ray energy of 20 keV, the correction due to the curved wave front is larger while the correction due to the near field effect caused by the vector field properties is smaller. This is because of the $1/k^2$ dependence in Eq. (20).

A generalized atomic scattering factor can be defined as a function of θ_i and r_i for XFH or MEXH with unpolarized incident beam

$$f_g(r_i,\theta_i) = f_i^S(r_i,\theta_i)(1+\cos^2\theta_i)/2$$

$$+\frac{e^{-ikr_i}}{2k^2}\left[(3\cos^2\theta_i-1)\frac{\partial}{\partial r_i}\eta(r_i,\theta_i)\right.$$

$$+\frac{\cos(2\theta_i)}{r_i}\frac{\partial^2}{\partial\theta_i^2}\eta(r_i,\theta_i)$$

$$+\sin(2\theta_i)\frac{\partial^2}{\partial r_i\partial\theta_i}\eta(r_i,\theta_i)$$

$$\left.+\frac{1-3\sin^2\theta_i}{r_i\tan\theta_i}\frac{\partial}{\partial\theta_i}\eta(r_i,\theta_i)\right]. \qquad (23)$$
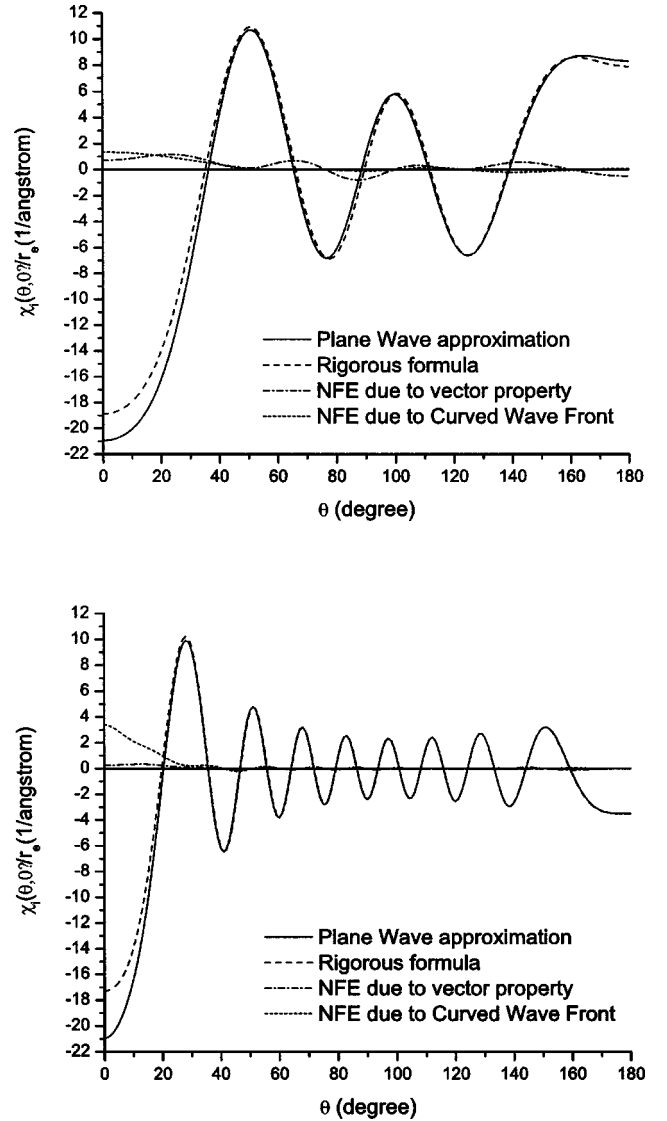
With this generalized atomic scattering factor, the simple

FIG. 5. (Color online) X-ray fluorescence hologram curves for a single pair of iron atoms separated by 2.4825 Å. Top: $E=6.4$ keV. Bottom: $E=20$ keV. Comparison is made with the plane wave approximation of Ref. 5. The contributions from the two kinds of the near field effects (NFE) to the hologram are also shown in the plots.

scalar form as of Eq. (2) can be used to calculate the hologram in XFH or MEXH with unpolarized incident beam. The near field effect caused by curved wave front is contained in the spherical wave ASF $f_i^S(r_i,\theta_i)$ while the near field effect caused by the vector property is presented in the four terms in the squared parentheses. Figure 6 shows the real and imaginary part of the generalized ASF for iron atom at 6.4 keV as function of θ_i with $r_i=2.4825$ Å. Since the generalized ASF is a slowly varying function of r_i and θ_i, it can be stored in a two dimension array at increment r_i and θ_i values. When calculating the x-ray hologram, the values of the generalized ASF at any r_i and θ_i values can be retrieved by interpolation. For MEXH with polarized incident beam [Eq. (21)], the generalized ASF can be divided into two parts f_g
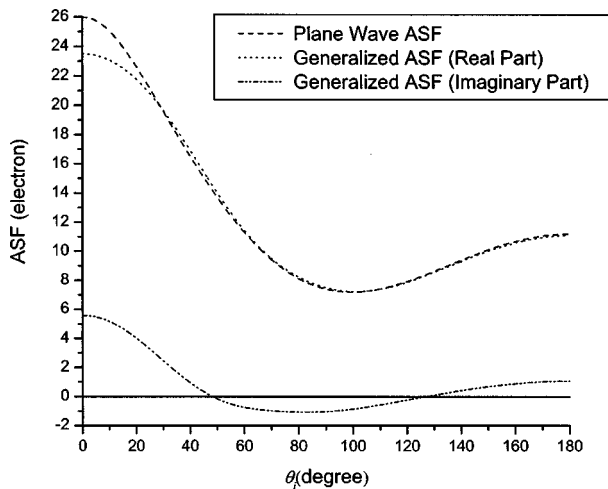
FIG. 6. The real and imaginary part of the generalized ASF with $r_i = 2.4825$ Å for iron atom and x-ray energy of 6.4 keV (Fe K_α lines). For comparison, the plane wave ASF multiplied by the polarization factor $(1 + \cos^2 \theta_i)/2$ is also plotted.

$= f_g^1(r_i, \theta_i) + f_g^2(r_i, \theta_i) \cos^2 \varphi_i$. In this paper we consider only the Thomson scattering. When x-ray energy is close to the absorption edge, the complex anomalous scattering factor should be added to the generalized ASF.

IV. CONCLUSION

In conclusion, the formalism for calculating the spherical wave ASFs from the radial electron distribution function or the tabulated plane wave ASF's is derived. The example calculation shows that the curved wave front correction to ASF's can be as large as 20 % of the plane wave ASF, depends on the source-scatterer distance and x-ray energy. This correction should be considered in all XFH or MEXH calcu-

lation. In addition, the near-field effects due to the vector property of the electromagnetic field is comparable to the curved wave front correction for low x-ray energies and must also be included for most of XFH calculation. For both kinds of near-field effects, the rigorous expressions for both XFH and MEXH are given. These expressions are essential for advanced reconstruction methods based on least-square-fitting algorithms.

There are other approximations in XFH theory, i.e., the single scattering approximation and the point dipole moment source approximation for the fluorescence atoms. Unlike photoelectron holography, in XFH the multiple scattering effects are generally negligible due to the small cross section for x-ray scattering. On the other hand, since only the inner shell fluorescence is used for XFH experiment, the size of the radiation source is also negligible. For example, the radius of the $1s$ shell of an Fe atom is 0.03 Å, which is only about 1.3 % of the nearest neighbor distance in a body centered cubic iron crystal and much smaller than the wavelength of iron K_α line. Therefore, the error caused by the point dipole moment field approximation should be one magnitude smaller than the corrections considered in this paper. Moreover, because of the spherical symmetry of the s-shell electron distribution, the dipole moment size effect should be isotropic and hardly detectable in XFH measurements.

[1] M. Tegze and G. Faigel, Europhys. Lett. **16**, 41 (1991).

[2] M. Tegze and G. Faigel, Nature (London) **380**, 49 (1996).

[3] T. Gog, P. M. Len, G. Materlik, D. Bahr, C. S. Fadley, and C. Sanchez-Hanke, Phys. Rev. Lett. **76**, 3132 (1996).

[4] J. J. Barton, Phys. Rev. Lett. **61**, 1356 (1988).

[5] B. Adams, D. V. Novikov, T. Hirot, and G. Materlik, Phys. Rev. B **57**, 7526 (1998).

[6] M. Tegze and G. Faigel, J. Phys.: Condens. Matter **13**, 10 613 (2001).

[7] H. C. Poon, D. Snider, and S. Y. Tong, Phys. Rev. B **33**, 2198 (1986).

[8] J. D. Jackson, *Classical Electrodynamics*, 2nd ed. (John Wiley & Sons, Inc., New York, 1975), p. 742.

[9] *International Tables for Crystallography*, Vol. C (Kluwer Academic Publishers, Dordrecht, 1992).

[10] C. Kittel, *Introduction to Solid State Physics*, 6th ed. (John Wiley & Sons, Inc., New York, 1986), p. 47.

[11] P. A. Doyle and P. S. Turner, Acta. Crystallogr. **24**, 390 (1968).

[12] D. Waasmaier and A. Kirfel, Acta Crystallogr., Sect. A: Found. Crystallogr. **51**, 416 (1995).

[13] F. N. Chukhovskii, D. V. Novikov, T. Hirot, and G. Materlik, Opt. Commun. **209**, 273 (2002).

[14] I. D. Feranchuk, L. I. Gurskii, L. I. Komarov, O. M. Lugovskaya, F. Burgäzy, and A. Ulyanenkov, Acta Crystallogr., Sect. A: Found. Crystallogr. **58**, 370 (2002).